

# SURFACE-GRATING-BASED DISTRIBUTED FEEDBACK LASERS FABRICATED USING NANOIMPRINT LITHOGRAPHY

J. Viheriälä, A. Laakso, M. Dumitrescu, J. Tommila, K. Haring,  
T. Leinonen, S. Ranta and M. Pessa

Optoelectronics Research Centre, Tampere University of Technology  
E-mail: Jukka.Viheriala@tut.fi, Antti.I.Laakso@tut.fi, Mihail.Dumitrescu@tut.fi

**Abstract**—Distributed feedback lasers with third-order surface gratings obtained by lateral corrugations of the ridge waveguide have been fabricated using low-cost nanoimprint lithography. The lasers, emitting in the 980 nm wavelength range exhibited stable single-longitudinal-mode operation with side-mode suppression ratios up to 50 dB.

**Keywords:** surface gratings, distributed feedback lasers, nanoimprint lithography.

## 1. INTRODUCTION

The conventional distributed feedback (DFB) edge-emitting laser (EEL) designs are based on incorporating a grating deep into the semiconductor epilayer structure, either inside the waveguide itself or close enough, so that the optical field is strongly coupled with the grating [1]-[3]. Such structures require two or more growth steps, bringing in the difficulties associated with the overgrowth, complicating the device fabrication and ultimately increasing the device cost. In order to avoid the problematic overgrowth we have used surface gratings, which consisted of lateral corrugations in the ridge waveguide (RWG), as illustrated in Fig. 1.

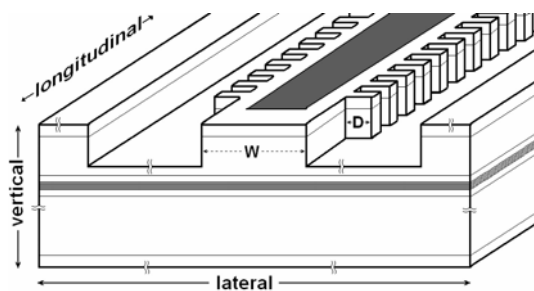


**Fig. 1.** Laterally-corrugated ridge waveguide (LC-RWG) structure.

In the laterally-corrugated ridge waveguide (LC-RWG) there is only a limited interaction between the grating and the carriers, which leads to more stable devices with better performances and increased reliability. Moreover, since the calculations and the preliminary experiments have shown that high-enough coupling

coefficients can be obtained without etching through the active region, the etching of the RWG corrugations has been stopped well above the active region, unlike in other approaches [4], thus avoiding the surface recombination at the etched lateral corrugation interfaces of the active region.

The LC-RWG structures have been fabricated in a single growth and processing sweep, increasing the yield and reducing the fabrication complexity. In order to enable a cost-effective development of the fabrication process (which requires numerous processing tests), the low-cost nanoimprint lithography has been used to define the process masks.

## 2. DEVICE FABRICATION

The epilayer structure for the laser was grown on an *n*-GaAs (100) substrate by solid-source molecular beam epitaxy. The active region, emitting at  $\lambda \approx 980$  nm, consisted of three 6 nm GaInAs quantum wells (QWs) with 8 nm GaAs barriers, embedded in an asymmetric 84/76 nm (*n*-/*p*-side) GaAs waveguide. A 30 nm lattice-matched GaInP etch stop layer was placed on top of the *p*-side waveguide layer. 1.2  $\mu$ m Al<sub>0.6</sub>Ga<sub>0.4</sub>As cladding layers and a heavily doped GaAs contact completed the epilayer structure.

UV-based nano-imprint lithography (UV-NIL), which enables pattern resolutions beyond the limitations set by the diffraction and scattering for the conventional techniques, was used for defining the corrugated ridge-waveguide. The master template for the UV-NIL stamps was fabricated by electron-beam-lithography (EBL) from a silicon-on-insulator wafer. This enables a very precise etching uniformity since the insulator layer is used as an etch stop for dry etching. The template was treated with 1H, 1H, 2H, 2H-perfluorodecyl-trichlorosilane in vapor phase to form an anti-adhesion layer and was subsequently replicated to UV-transparent three-layer silicone-based stamps. The use of these stamps to create the process masks onto the

epiwafer enables multiple processes based on a single master template (which is the most expensive part of the process).

The fabrication of the three-layer silicone-based stamps started with a thin layer of polydimethylsiloxane (PDMS) spun on the master template. Then a thin flexible glass plate was placed onto the uncured PDMS and the ensemble was cured. After curing, the glass-hard-PDMS ensemble was separated from the master template and attached to a thick slab of soft PDMS. The use of the thin glass layer prevents the lateral stretching of the patterns while maintaining the stamp soft and flexible. The softness and flexibility enable the three-layer stamps to adapt to wafer-scale nonflatness (i.e. particles, curvature, waviness etc.), making possible full-wafer imprinting with low pressure (50 - 500 mbar). The flexibility also greatly eases stamp separation after imprinting (which is desired when working with fragile wafers). The UV-transparency of the stamps offers the possibility to use low viscosity UV-curable polymers. The low viscosity promotes fast process throughput and, because the resist is UV-cured, the imprint sequence does not require heating (which may cause replication inaccuracies due to different thermal expansion coefficients).

The ridge and grating were defined by etching a corrugated pool on both sides of the ridge waveguide. The primary etch mask was a 200-nm thick  $\text{SiO}_2$  layer, which was patterned with the three-layer UV-NIL stamp and a lift-off process. The lift-off mask was prepared from 80 nm of polymethyl methacrylate (PMMA), 10 nm of Ge and a layer of NIL-resist. EVG 620 UV-mask aligner, equipped with NIL tooling was used to pattern and cure the resist. The residual resist layer, left on the imprinted areas, was dry etched, followed by two additional etch steps to penetrate the Ge and PMMA layers. Aluminum was evaporated and the PMMA layer was dissolved leaving Al only onto desired areas. Fig. 2 illustrates the accuracy of the replication process from master template to Al etch mask.

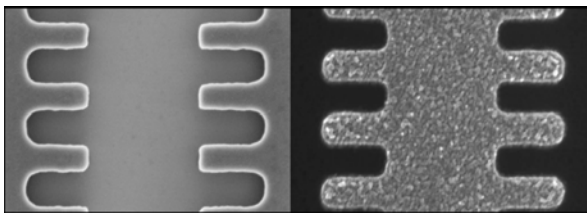


**Fig. 2.** Master template profile (left panel) and replicated Al etch mask (right panel).

The remaining Al mask was used to etch  $\text{SiO}_2$  and, subsequently, the  $\text{SiO}_2$  was used to etch the semiconductor all the way to the etch-stop layer. Although a first-order grating mask (with the period in the 150 nm range) is easily achievable by the UV-NIL based process (Fig. 3 shows imprints obtained by UV-NIL, with linewidths below 30 nm), a third-order grating (with period around 450 nm) was imprinted for the fabrication of the DFB lasers.

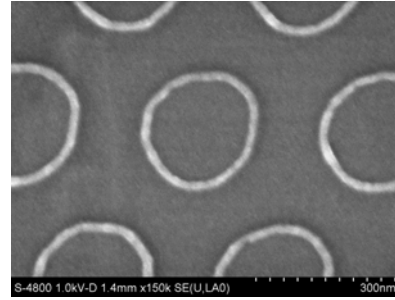


**Fig. 3.** Imprints obtained by UV-NIL and PDMS stamp, with linewidths of about 20 nm.

The use of wider third-order gratings was due to the fact that the etching depth (of about 1700 nm) together with first-order gratings would have implied an aspect ratio for which the accurate processing of the gratings would have been difficult. The smaller etch aspect ratio associated with third-order grating with 50% filling factor ( $\sim 1700/225$ ) enabled more accurate processing results, illustrated in Fig. 4.

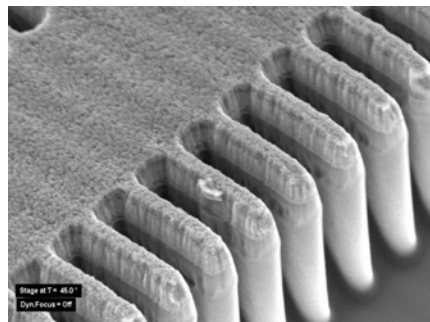


**Fig. 4.** SEM image of the third-order laterally-corrugated ridge waveguide grating.

Different values for the width of the un-etched central part of the ridge ( $W$  in Fig. 1) and for the depth/extension of the lateral corrugation ( $D$  in Fig. 1) have been tested, with similar processing results for  $W=0.8-2$  and  $D=0.5-1.5$   $\mu\text{m}$ . After etching the laterally-corrugated RWG, the top side of the wafer was passivated with  $\text{SiO}_2$ . The  $\text{SiO}_2$  layer was subsequently opened on top of the

ridge for current injection. No phase-shift section was used in the DFB structure since we have found out that its presence is detrimental to the laser characteristics when third-order gratings are employed. In the end of the wafer-level processing the wafer was thinned and metallized on both sides. The bars/chips were cleaved/separated from the wafer and the front/back facets were antireflection/high reflection coated. The chips were packaged on copper mounts *p*-side up.

### 3. DEVICE CHARACTERIZATION

Fig. 5 shows the current-light-voltage (*I-L-V*) curves and the optical spectrum measured at 10 mW for a 600- $\mu\text{m}$  long DFB EEL with  $W=1.5\ \mu\text{m}$  and  $D=0.5\ \mu\text{m}$ . The device exhibited 30 mA threshold current, 0.34 W/A slope efficiency and 50dB side-mode suppression-ratio (SMSR) at 10mW, when operated at 10°C. These characteristics can be significantly improved since the epilayer and device structure have not been optimized. Most of all, the relatively high voltage and series resistance are related to p-contact, reduced contact stripe width and un-optimized epilayer structure and doping profile.

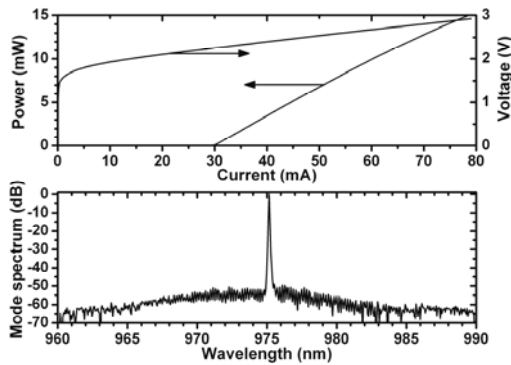


**Fig. 5.** Measured *I-L-V* curves and emission spectrum (at 10 mW) for 600- $\mu\text{m}$  long LC-RWG DFB laser.

Smooth/conventional RWG Fabry-Perot (FP) EELs have been simulated, fabricated and experimentally characterized in order to evaluate the effects of the RWG lateral grating on the device performances. The upper panel of Fig. 6 presents simulated *LI*-curves for un-coated 2.5  $\mu\text{m}$  wide and 600  $\mu\text{m}$  long conventional RWG FP EELs. The simulated threshold currents were 12, 12.5, 13 and 13.7 mA, while the simulated slope efficiency values were 0.8, 0.62, 0.53 and 0.39 W/A for internal loss coefficient values of 10, 15, 20 and 25  $\text{cm}^{-1}$ , respectively. Experimentally characterized conventional RWG

FP EELs with similar ridge geometry and cavity length had threshold currents of 10-15mA and slope efficiencies around 0.4-0.5, matching best the simulations with  $\alpha=20\text{cm}^{-1}$ . The lower panel of Fig. 6 shows the simulated FP mode spectrum at 35mA for  $\alpha=20\text{cm}^{-1}$ .

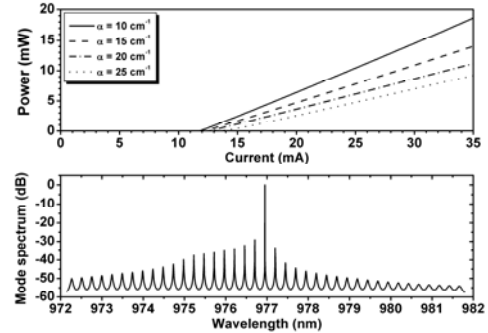


**Fig. 6.** Simulated *LI*-curves for  $2.5 \times 600\ \mu\text{m}$  Fabry-Perot RWG EEL with different loss coefficients (upper panel) and simulated emission spectrum at 35mA for  $\alpha = 20\text{cm}^{-1}$  (lower panel).

The fabricated LC-RWG exhibited a 55% decrease in the slope efficiency, a 130% increase in threshold current and a 92% (24 dB) increase in the SMSR (see Fig. 7), as compared to the simulated FP RWG EEL with  $\alpha=20\ \text{cm}^{-1}$  and the same ridge width and etching depth. These variations can be attributed mainly to increased surface recombination of the carriers, to a decreased QW confinement factor (induced by reduced effective ridge contrast) and to increased radiative and scattering losses. While the LC-RWG EEL obviously has more stable single-mode operation and a higher SMSR, as compared with FP RWG EEL, the simulations have indicated that the other DFB laser characteristics can be significantly improved by epilayer and device structure optimizations.

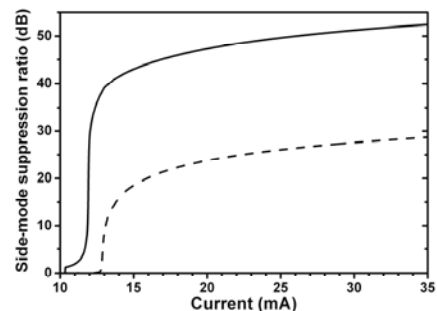


**Fig. 7.** Simulated SMSR for the LC-RWG DFB-laser (solid line) and for the conventional FP RWG laser with the same ridge width and thickness of the un-etched cladding (dashed line).

Fig. 8 shows emission spectra from the LC-RWG DFB EEL, measured at different operating temperatures. The grating resonance shift with temperature was 0.08 nm/K over ambient temperature from -15 to +15 °C. For the grating period of 440 nm the best performances were obtained at lower temperatures (when the grating resonance is well-aligned with the gain peak), indicating that the grating period should be increased for optimum performance at room temperature.

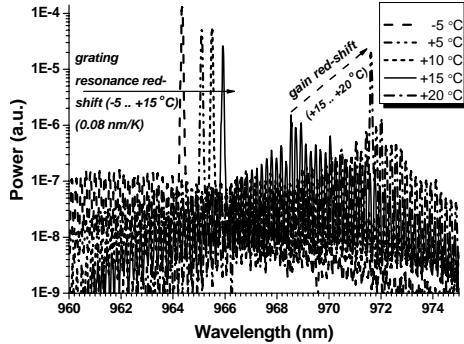


Fig. 8. Measured LC-RWG DFB laser emission spectra at different temperatures.

Since the gain peak red-shifts more than the grating resonance with increasing temperature, a significant side-mode, aligned with the gain peak, appears at higher temperatures (seen at about 968.5 nm in the 15 °C emission spectrum of Fig. 8). At even higher ambient temperatures, when the gain at the grating resonance becomes too small, the device ceases to operate in the DFB regime and the emission spectrum becomes similar with the one of a FP device (the 20°C emission spectrum of Fig. 8). The LC-RWG DFB EEL peak gain red-shift with temperature (0.6 nm/K) is significantly higher than the peak gain red-shift for a conventional RWG FP EEL measured in pulsed-operation regime (0.3 nm/K), indicating that the LC-RWG DFB device is substantially self-heating. Therefore, better thermal management of the device would significantly decrease the rate of the wavelength shift with temperature.

Taking into account the need for fine-tuning of the emission wavelength, we have also investigated the current-tuning capabilities of the LC-RWG DFB devices. Fig. 9 shows the emission spectra at different bias currents, indicating that a fine current-tuning of the emission wavelength (with a 0.033 nm/mA rate) can be achieved.

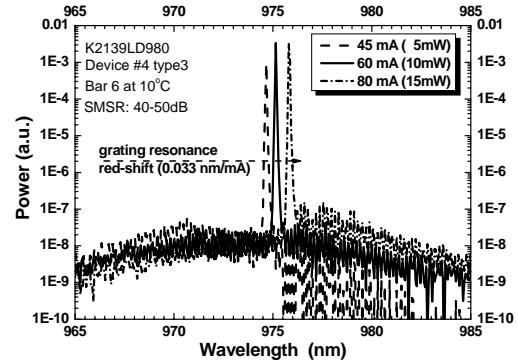


Fig. 9. Measured LC-RWG DFB laser emission spectra at different bias currents.

## 4. CONCLUSIONS

DFB lasers with laterally-corrugated ridge waveguide third-order gratings have been fabricated using low-cost UV nanoimprint lithography. The fabrication process, consisting of a single growth and processing sweep, avoids the difficulties and drawbacks associated with overgrowth and can be applied to different wavelengths and (with minimal changes) to different underlying epilayer structures. 600µm long LC-RWG DFB lasers with 2.5µm wide corrugated ridge ( $W+2*D=1.5+2*0.5\mu\text{m}$ ) exhibited 30mA threshold current, 0.34 W/A slope efficiency and 50dB side-mode suppression-ratio at 10mW, when operated at 10°C. Smooth 0.08nm/K temperature tuning over more than 30 degrees and smooth 0.033nm/mA current tuning have been experimentally achieved. The simulations indicate that the device performances can be significantly improved by epilayer and device structure optimizations.

## References

- [1] J. Buus, "Single Frequency Semiconductor Lasers", *SPIE Optical Engineering Press*, Bellingham, Washington, 1991.
- [2] R. Nagarajan, "Distributed Feedback Lasers", *Wiley Encyclopedia of Electrical & Electronics Engineering*, Wiley & Sons, 1999, pp.705-714.
- [3] A.C. Abare, S.P. Denbaars, L.A. Coldren, "Distributed feedback laser diodes employing embedded dielectric gratings located above the active region", *IEICE Trans. Electronics*, vol. **E83C-4**, Apr. 2000, pp. 560-563.
- [4] K. Mathwig, W. Kaiser, A. Somers, J.P. Reithmaier, A. Forchel, K. Ohira, SW. M. Ullah, S. Arai, "DFB Lasers With Deeply Etched Vertical Grating Based on InAs-InP Quantum-Dash Structures", *IEEE Phot. Techn. Lett.*, vol. **19**(5), March 2007, pp. 264-266.